DESIGN OF A CERAMIC HEAT EXCHANGER FOR HIGH TEMPERATURE APPLICATIONS USING SIMULATION TECHNIQUES

Paulo Eduardo Batista de Mello, pmello@fei.edu.br
Gustavo Henrique Bolognesi Donato, gdonato@fei.edu.br
Departamento de Engenharia Mecânica – Centro Universitário da FEI
Av. Humberto de Alencar Castelo Branco, 3972, São Bernardo do Campo – SP
09850-901

Abstract. *There is a potential demand for heat exchangers capable of supporting working temperatures well above 900°C. Many different studies in the literature consider these components as critical for the implementation of externally fired gas turbines (EFGT) and externally fired combined cycles (EFCC). It is common sense that ceramics are the only alternative for the construction of these heat exchangers, but most part of the literature about heat exchangers usually considers only metallic materials for its construction. Consequently, the design of ceramic heat exchangers is not trivial and represents an actual technical challenge. In addition, different heat transfer modes are present simultaneously and structural integrity considerations also become highly important due to the thermal stresses originated from high temperature gradients combined to the brittle fracture behavior of engineering ceramics. As a step in this direction, the present work presents the design of a ceramic heat exchanger using CFD and finite element structural simulations. The heat exchanger designed presents small dimensions in order to make it easier to construct a prototype and test it in the future.*

Keywords*: ceramic heat exchanger, EFGT, EFCC.*

1. INTRODUCTION

There is a potential demand for heat exchangers capable of supporting working temperatures well above 900°C. In the literature, these heat exchangers are known as HTHE (high temperature heat exchangers) and ceramic materials are the actual natural choice for the task. One review about HTHEs is presented by Sunden (2005), where possible applications are discussed.

One of the promising applications for HTHEs is in the power industry, because they would turn possible the implementation of EFGT (externally fired gas turbines) and EFCC (externally fired combined cycles). The typical arrangement of the components of one EFGT cycle is shown in Fig. 1. As stated by Kautz and Hansen (2007), the key component in the cycle is the HTHE, because the other components are standard parts. In both of these cycles the combustion flue gases don't pass through the turbine so that other fuel than gas can be used, like biomass or coal.

One ceramic plate-fin HTHE was designed by Fischedick et al (2007) for 50kWth and many important design considerations were evaluated, such as: the choice of the ceramic material; structural integrity of the heat exchanger; thermal design; pressure drop introduced by the heat exchanger, and others that will be addressed in the present study.

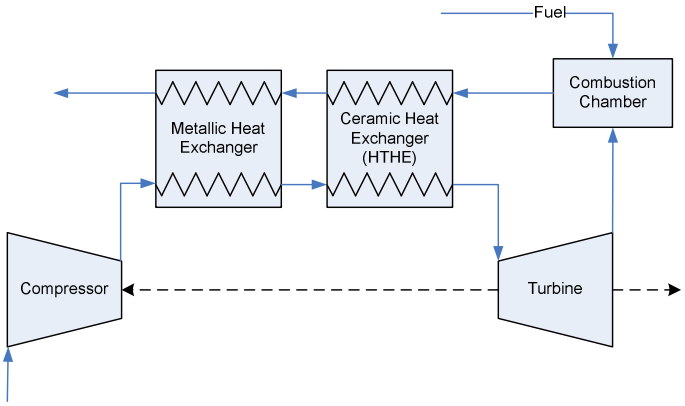

Figure 1. Typical arrangement of the EFGT components.

Pressure drop produced by the heat exchanger deserves special attention during design stage because it reduces the thermal efficiency of the cycle (Kautz and Hansen, 2007).

The challenge in the design of a ceramic HTHE for power applications is to achieve high effectiveness without producing high pressure drop. It is considered a difficult task since the same heat capacity rate is observed in both sides of the heat exchanger. At the same time, structural integrity of the equipment must be assessed in order to guarantee or even increase its life cycle, while keeping safety by predicting and avoiding catastrophic failure.

2. OBJECTIVES

The design of a ceramic heat exchanger is presented and discussed in the present work. The design is conducted considering a very small heat exchanger that could be tested in a laboratory bench work, producing useful data for the validation of the presented design methodology. The final prototype should have external dimensions smaller than 100 mm.

The design of the heat exchanger is aiming at a particular application: the EFGT, but it doesn't consider significant pressure differences between the hot and cold sides, which would introduce one extra difficulty for the future experimental tests. Besides, other characteristics of the application are maintained: air is the fluid in both sides of the heat exchanger and the flow rate is the same for the hot and cold sides. This condition, as discussed later, will present limitations to the effectiveness that can be obtained for the heat exchanger.

The thermal design of the heat exchanger is conducted using CFD simulations. The temperature distribution in the walls of the ceramic material is then used as input for structural simulations using the finite element method.

3. MATERIAL SELECTION

The material selection for the construction of a ceramic heat exchanger to be used in the power industry should consider many factors, some of them discussed by Fischedick et al (2007). In the present work, considering the validation purposes of the prototype to be constructed, some of those factors are less important and can be neglected. So, sintered alumina (Al_2O_3) was selected based on its low cost, high thermal stability and feasible construction. Once the present design approach is experimentally validated, it will be easy to change material properties and evaluate the influence over the heat exchanger's performance and behavior.

The main thermal and mechanical properties considered for the alumina are presented by Table 1. Here, k represents the thermal conductivity, E represents the elastic modulus, ν is the Poisson's ratio, σ_{uts} is the ultimate tensile strength (adopted balanced for tension and compression $\sigma_{uts}=\sigma_{ucs}$) and α is the thermal expansion coefficient from 0 ºC. In all analyses that follow, material is assumed to be isotropic and homogeneous.

Table 1 – Thermal and mechanical properties considered for the Sintered Alumina (Al_2O_3) at 500°C (NIST, 2010).

k [W/m K]	E [GPa]	N	$\sigma_{uts}=\sigma_{ucs}$ [MPa]	α [10^{-6} K^{-1}]
11.4	390	0.237	267	7.1

4. THERMAL DESIGN

In the work of Fischedick et al (2007), the thermal design of the HTHE was conducted by using correlations for the Colburn and friction factors for offset strip fins. These correlations were obtained from experiments by Manglik and Bergles (1995).

The present work uses CFD simulations for the thermal design task. This choice can be justified by the possibility of considering the heat conduction in the ceramic material coupled with the convective heat transfer, technique known as conjugate heat transfer. This type of simulation is particularly important since it can provide the temperature distribution in the ceramic material as a result that can be used as input to the structural design.

The number of transfer units (NTU) method is used for the present analysis and design. The theory related to NTU can be found in many texts from literature. It states that the effectiveness ε depends on the number of heat transfer units NTU and the heat capacity rates of the hot and cold flows C_r. This dependence is summarized by Eq. (1).

$$\varepsilon = \varepsilon(NTU, C_r) \tag{1}$$

The number of transfer units (NTU) and the ratio between heat capacity rates are given by Eq. (2) and (3), respectively.

$$NTU = \frac{UA}{C_{min}} \tag{2}$$

$$C_r = \frac{C_{min}}{C_{max}} \tag{3}$$

Here, U is the overall heat transfer coefficient, A is the heat transfer area, and C_{min} and C_{max} are the minimum and maximum capacity rates.

The literature presents many relations and graphs that permit to obtain the dependence summarized by Eq. (1) for many different configurations of heat exchangers. The present analysis is focused on cross-flow heat exchangers. Figure 2 graphically presents the effectiveness for this particular configuration. It is important to observe that the condition where both heat capacity rates are equal (and $C_r = 1$) is the condition that demands more heat transfer area in order to achieve a given effectiveness.

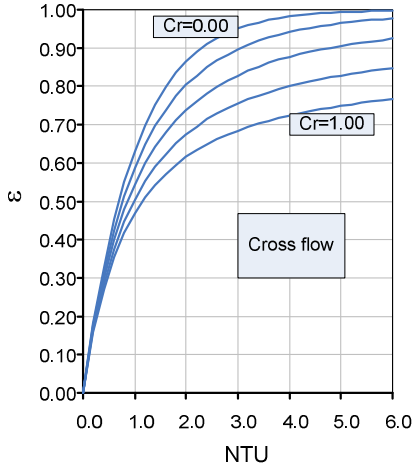

Figure 2. Effectiveness of a cross-flow heat exchanger.

The heat exchanger designed in the present work is very similar to the one presented by Fischedick et al (2007), but its dimensions are much reduced, for the reasons already commented in the design objectives section. The heat exchanger is formed by ceramic plates that are stacked. The geometry of the ceramic plates can be seen in Fig. 3 and its dimensions were a result of the following criteria: the thickness of any plate region should not be less than 5 mm; the external dimensions of the mounted heat exchanger should be smaller than 100 mm.

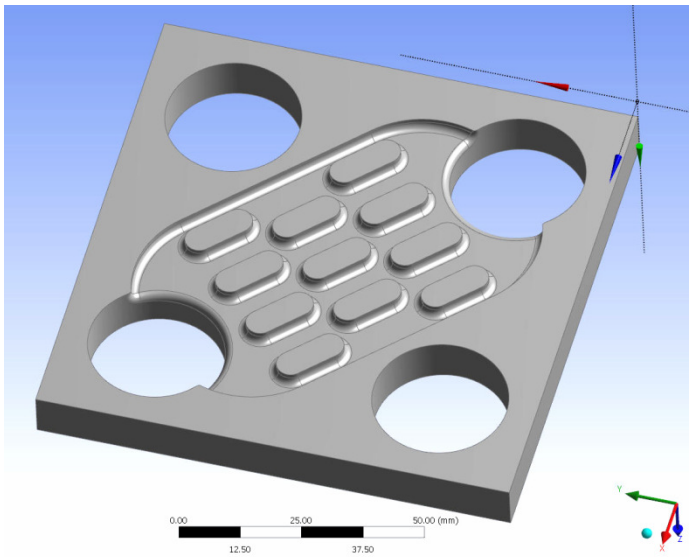

Figure 3. Geometry of the ceramic plates that are stacked in order to form the heat exchanger.

4.1. CFD Simulations

All the CFD simulations were conducted using CFX-12 computer code. This computer code is well known and detailed description of its features and models are omitted here for brevity.

The convergence criteria was set to RMS of the residuals lower than 5×10^{-5}. The high order interpolation scheme was used. The Reynolds number, based on the 5.0 mm channels shown in Fig. 3, is between 200 and 1000, depending on the flow rate. Therefore, no turbulence model was needed. The density variation with temperature is very significant for the application considered herein and it was considered in the simulations with ideal gas model.

One grid influence test was conducted with 7 different grids, with constant wall temperature as boundary condition, considering only the air flow through the channels (without conjugate heat transfer). The number of elements in the grids varied from 1.8 to 2.7 millions. The results have not shown asymptotic behavior, but the difference observed

between the highest and lowest heat transfer rate was smaller than 2.8% (182.4 W and 187.5 W respectively). It produced differences over the effectiveness of 3.7%, considered satisfactory.

The comprehension of the behavior of a heat exchanger under ideal conditions is valuable, and numerical simulations are very useful for this purpose. Initial simulations were conducted considering the ideal condition where the temperature of the wall is constant. This approach was useful for the determination of an adequate flow rate due to the dependence of the number of transfer units (NTU) over flow rate. One typical distribution of the local heat transfer coefficient can be seen in Fig. 4. The distribution obtained is consistent with theory, showing higher heat transfer in regions where a new boundary layer is formed.

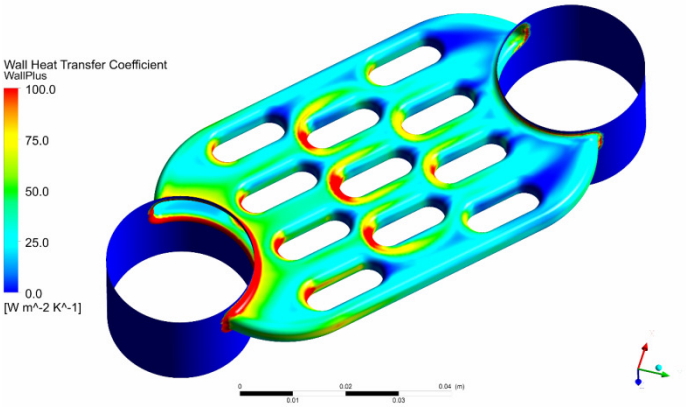

Figure 4. Contour of local heat transfer coefficient (air is flowing from left to right; walls at constant temperature).

The results obtained with a typical simulation, with constant temperature in the wall, are presented in table 2. For this ideal condition the overall heat transfer coefficient is equal to the average heat transfer by conduction.

Table 2: Results obtained with a typical simulation, with constant temperature in the wall (T_{wall} = 700°C; T_{in} = 30°C) and mass flow rate of 5.0×10^{-4} kg/s.

Q [W]	Tout [°C]	U [W/m^2 K]	ε [-]	NTU [-]
182.4	392.6	37.9	0.541	0.779

In table 2, the heat transfer rate Q and the temperature at the outlet Tout are obtained directly from the CFD simulation. The effectiveness is obtained with Eq. (4).

$$\varepsilon = \frac{Q}{Q_{max}} = \frac{Q}{C_{min}\left(T_{wall} - T_{in}\right)} \tag{4}$$

The NTU, for this ideal case where the wall temperature is constant, can be obtained with Eq. (5), which is valid for any heat exchanger configuration, when $C_r = 0$.

$$NTU = -ln\left(1-\varepsilon\right) \tag{5}$$

The importance of these preliminary simulations with constant temperature in the wall is evident with the careful inspection of Fig. 2. It reveals that the flow rate used for the simulation presented in table 1 is too high. Even with C_r = 0, the effectiveness obtained was only 0.54. Under real conditions, where C_r is close to unity, the effectiveness should be significantly lower. It suggests that the effect of the flow rate over the effectiveness could be evaluated with the ideal model before dealing with the much demanding model, using conjugate heat transfer.

Following this approach, a series of simulations with different flow rates was conducted. When the flow rate is reduced, the overall heat transfer coefficient U and the heat capacity rate C_{min} decrease. Due to this behavior, it is not obvious the effect of the flow rate over NTU. But the graph of Fig. 5, which summarizes the results, shows clearly that NTU increases when flow rate is reduced. In other words, C_{min} decreases faster than U when the flow rate is reduced, at least for the heat exchanger considered here.

Of course, another option to increase NTU would be to increase heat transfer area, but it is not in agreement with the objectives of the present work, considering the limitations imposed to the size of the heat exchanger. The effectiveness, for the ideal case, varied from 0.96 to 0.54, when the flow rate is increased from 0.5×10^{-4} kg/s to 5.0×10^{-4} kg/s.

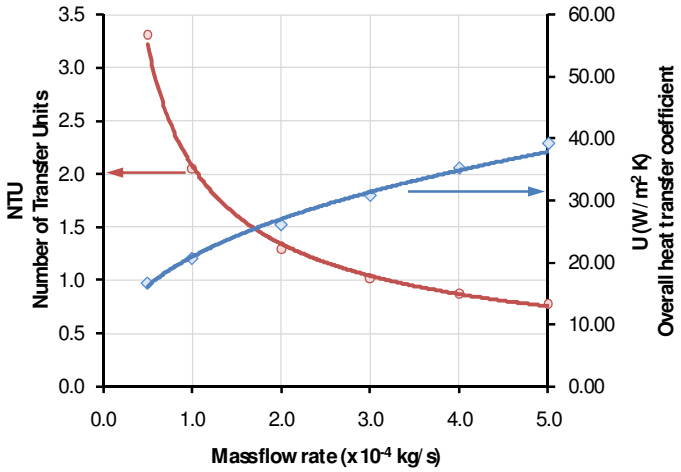

Figure 5. The effect of flow rate over the NTU and U, for the ideal case with constant temperature in the wall.

Conjugate heat transfer simulations were conducted including the effect of heat conduction in the ceramic walls. The steady state simulations considered the heat conductivity of alumina k = 11.4 W/m K, according to data from NIST (2010). Figure 6 shows the stacked arrangement of the plates. The geometry of each plate was already shown in Fig. 3. Only one pair of plates was simulated and periodicity boundary conditions were used in order to approximate the stacked plate arrangement. Periodic boundary condition means that, for calculation purposes, the bottom side of the pair of plates is in contact with the top side of an adjacent pair. This boundary condition is used only for the solid domain.

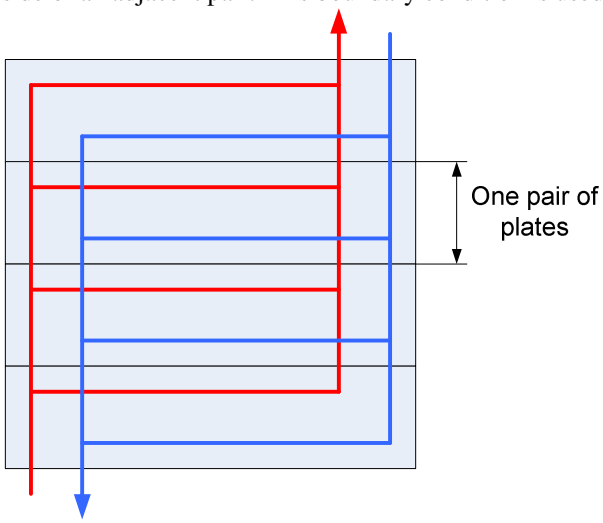

Figure 6. Scheme of the stacked ceramic plates. Only one pair of plates is considered in the simulation.

For the fluid domains, temperatures and flow rates are imposed in the inlets of the heat exchanger. Different flow rate conditions were simulated, but maintaining equal flow rates on cold and hot sides for each condition. Temperatures imposed to the inlet flows of the cold and hot sides are respectively 30°C and 1000°C.

The most important result of each simulation is the temperature of the air leaving the heat exchanger, in hot and cold sides. These results allow the calculation of a series of derived results: effectiveness, NTU, among others. Effectiveness is calculated using Eq. (6).

$$\varepsilon = \frac{Q}{Q_{max}} = \frac{Q}{C_{min}\left(T_{in,hot} - T_{in,cold}\right)} \tag{6}$$

NTU can be calculated using Eq. (7), for the case of a cross flow heat exchanger with both fluids mixed and $C_r = 1$, available from Kays and London (1984).

$$\varepsilon = \frac{NTU}{\frac{2\,NTU}{1 - exp\left(-\,NTU\right)} - 1} \tag{7}$$

Figure 7 summarizes the results obtained. It is interesting to compare these results with the ideal results of Fig. 5. This comparison reveals a substantial reduction in the overall heat transfer coefficient. The effectiveness of the cross flow heat exchanger is significantly reduced if compared to the previous ideal case. It varied from 0.47 to 0.37, when the flow rate is increased from 1.0×10^{-4} kg/s to 3.0×10^{-4} kg/s.

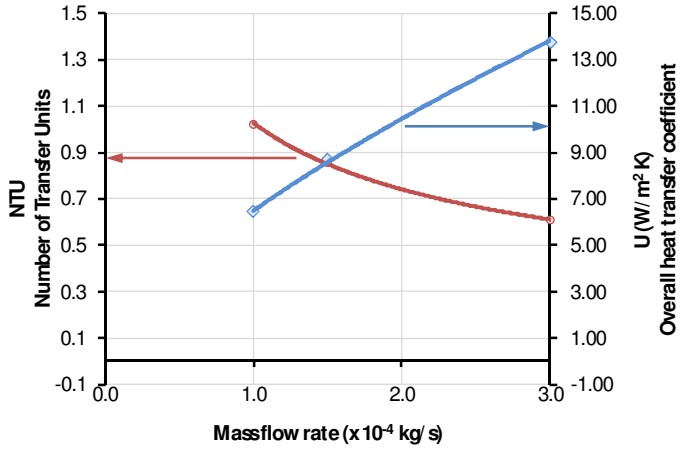

Figure 7. The effect of flow rate over the NTU and U, for the simulations considering the conjugate heat transfer.

Equation (8) helps to understand the strong reduction in the overall heat transfer coefficient comparing the ideal case with the conjugate heat transfer case. For the ideal case with constant temperature in the wall, the overall heat transfer coefficient is equal to the heat transfer coefficient by convection. When the conjugate heat transfer is considered, there is a sum of resistances, resulting in a strong decrease in the coefficient U, as presented by Eq. (8).

$$\frac{1}{U\,A} = \frac{1}{h_{hot}\,A\,\eta_{fin}} + R_w + \frac{1}{h_{cold}\,A\,\eta_{fin}} \tag{8}$$

This reduction in coefficient U cannot be attributed to the thermal resistance of the wall, though. It is a combination of factors: the cross flow arrangement, the efficiency of the fins and heat conduction in the walls.

It is tempting to attribute the weak thermal performance of the heat exchanger to the thermal resistance of the walls, because the ceramics present low thermal conductivity if compared to metals. However, it is not the case for the heat exchanger considered herein. The simulations were repeated with modification in the thermal conductivity of the material (multiplied by 100), and the result obtained was almost the same. It allows concluding that the low overall heat transfer coefficient should not be attributed to the properties of the ceramic, but to the low convective heat transfer coefficients obtained with the laminar flow. One counter flow arrangement is another option to increase the performance.

Another important result obtained from the conjugate heat transfer simulation is the temperature distribution in the ceramic plates (Fig. 8). This result allows structural integrity detailed assessment of the plates when submitted to rigorous thermal stresses.

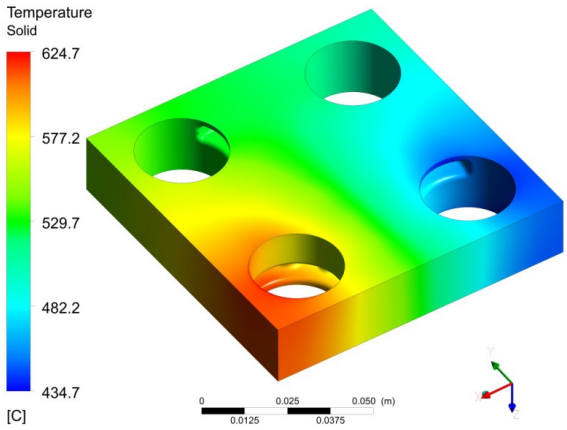

Figure 8. Temperature distribution in the ceramic plates (°C).

The thermo structural design discussed bellow is based in the temperature distribution obtained with air flow rates equal to 1.0×10^{-4} kg/s.

5. THERMO STRUCTURAL DESIGN

Engineering ceramics are of great interest for the design and construction of high temperature heat exchangers as already mentioned. However, its design is nowadays considered a technological challenge due to the high brittleness of ceramic materials and the exposure to severe loadings. This kind of equipment has to stand severe pressure, steady state and transient thermo mechanical loadings, with lifetime of approximately 10^5 hours for the use in power plants (Fischedick et al, 2007). Consequently, adequate material's selection and structural design and integrity assessments are mandatory.

The heat exchanger studied here was designed with all internal radii as large as possible to avoid geometrical discontinuities and minimize resulting stress levels, as was presented by Fig. 3 and 4. In addition, it can be realized that symmetry exists in the flow direction, which shall reduce thermal stresses. Therefore, due to the complex geometry, the present work applied the finite element method (FEM) to obtain the stress fields for structural integrity evaluation. The detailed computational procedures will be presented in the next section.

Design against brittle fracture using ceramic materials can be conducted based on conventional fracture criteria (e. g.: Maximum Normal, Mohr-Coulomb) (Dowling, 1999) or on fracture mechanics theory, which considers the presence of crack-like defects in the structure (Anderson, 2005). The latter can provide more detailed and accurate results, but demands a complete characterization of material properties including distribution and size of microdefects, which is beyond the frame of this paper. From a mechanical and macroscopic point of view, however, the use of conventional fracture criteria applicable to brittle materials is perfectly capable of predicting the structural integrity based on available mechanical properties, such as presented by Table 1. In this case, both Maximum Normal and Mohr-Coulomb criteria were considered, which will be briefly discussed.

The maximum normal stress fracture criterion is the simplest fracture criterion and preconizes that failure is expected when the largest principal stress reaches the uniaxial ultimate tensile strength (σ_{uts}) of the material, as presented by Eq. (9).

$$\sigma_{ef} = max\left(|\sigma_1|,|\sigma_2|,|\sigma_3|\right) = \frac{\sigma_{uts}}{SF_{mn}} \tag{9}$$

Here, σ_{ef} represents an effective stress, σ_1, σ_2 and σ_3 are principal stresses and SF_{mn} represents the safety factor against brittle fracture based on the maximum normal stress criterion. Absolute values for the principal stresses are considered so that compressive principal stresses are equally assessed. In addition, the ultimate tensile strength of the material is considered the same in tension and compression, which keeps the applicability of Eq. (9).

The maximum normal stress criterion gives accurate failure predictions as long as the largest normal stress is tensile. If large compressive principal stresses are characterized, failure predictions can be highly inaccurate. The randomly oriented microscopic cracks commonly found in brittle materials cannot support significant tensile stress (acting as stress raisers). On the other hand, they have little sensitivity to compressive stresses (crack surfaces are pressed against each other), providing higher strengths in compression for brittle materials. Also, failure usually occurs on planes inclined to the planes of principal normal stress and more nearly aligned with planes of maximum shear. Therefore, alternative criteria which include this phenomena (i. e.: the Mohr-Coulomb fracture criterion) deserve investigation in the present work.

This criterion predicts that the failure will occur on a given plane in the material when a critical combination of shear and normal stress acts. This condition is met if one of the statements presented by Eq. (10) is satisfied,

$$\begin{aligned}
&|\sigma_1 - \sigma_2| + m\cdot(\sigma_1 + \sigma_2) = 2\cdot\tau_u \\
&|\sigma_2 - \sigma_3| + m\cdot(\sigma_2 + \sigma_3) = 2\cdot\tau_u \\
&|\sigma_3 - \sigma_1| + m\cdot(\sigma_3 + \sigma_1) = 2\cdot\tau_u
\end{aligned} \tag{10}$$

where τ_u is the pure shear stress necessary to cause fracture and m characterizes the material's ultimate strength in tension and compression in the form

$$m = \frac{\sigma_{ucs} + \sigma_{uts}}{\sigma_{ucs} - \sigma_{uts}} \tag{11}$$

6. FINITE ELEMENT MODELS

Detailed thermo-structural finite element analyses were performed using Ansys Workbench 12.0.1 and Ansys Mechanical 12.0.1 computer codes, with linear-elastic constitutive model in small geometry change (SGC) setting (Bathe, 1996). The utilized material properties were presented by Table 1. Figure 8 presents the geometry considered, which comprehends the plate showed in Fig. 3 covered in the upper and lower parts by additional half-plates, in order to configure one "block" of the stacked heat exchanger (see Fig. 6 for better comprehension).

All finite element meshes were created using 3D ten-node linear strain tetrahedral elements, with selective refinement based on curvature criteria. In order to guarantee numerical convergence and accurate stresses, different meshes were created with increasing refinements near the critical regions. Were tested 4, 5, 6 and 8 nodes to describe the smaller radii, and stable stress levels were obtained (with variation of stresses under 3% for 33% increase in refinement) for a minimum of 6 nodes per rounded corner, as can be realized in Fig. 9 for the localized maximum principal stresses. Figure 10, in its turns, present the final mesh used for the computations (with 8 nodes per rounded corner), comprehending 195,953 nodes and 927,255 3D elements.

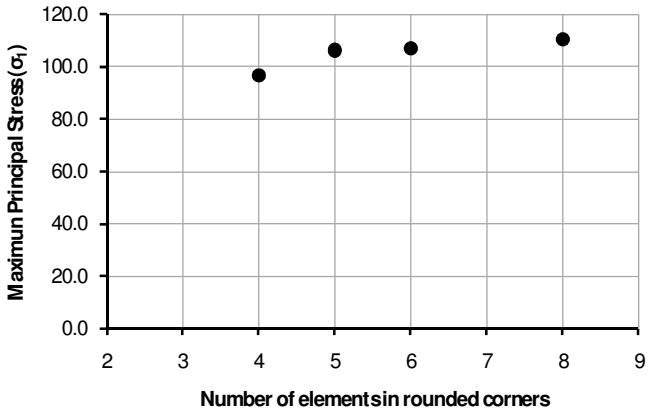

Figure 9. Mesh refinement analysis showing stable principal stress values using a minimum of 6 tet-10 3D elements in rounded corners.

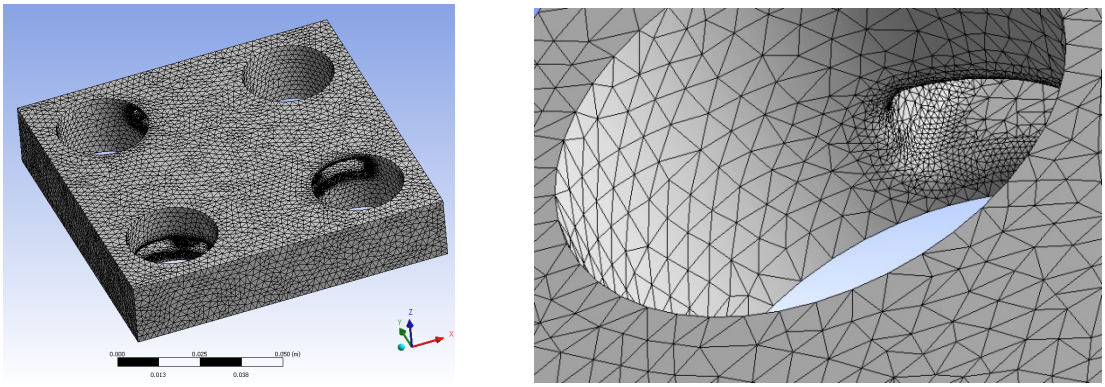

(a) (b)

Figure 10. Final mesh used for the computations, comprehending 195.953 nodes and 927.255 3D tet-10 elements. (a) Were used 8 nodes in rounded corners. (b) Detail of the final mesh used for the computations. It can be realized the curvature-based increased refinement.

The heat exchanger has laboratory and thermal efficiency validation purposes and is, consequently, not expected to work with the high pressures found in real turbines. Therefore, the temperature distribution (which is responsible for significant thermal stresses) is defined as the main boundary condition for the structural finite element model. This temperature distribution was provided by the conducted CFD simulations and was presented by Fig. 8.

Figures 11 and 12 present some obtained results in terms of displacement fields and principal stresses. Figure 11 shows that the displacement fields in the upper and lower parts of the analyzed structure are essentially similar, which is a positive result for the intended multilayer configuration. In addition, the critical region was identified near a rounded corner (see Fig. 11), with principal stresses presented by table 3 (maximum value of σ_1 = 111.0 MPa - tensile stress).

Table 3: Principal stresses identified in the critical region.

Principal stress	σ_1 [MPa]	σ_2 [MPa]	σ_3 [MPa]
Values-critical region	111.0	7.90	5.34

(a) (b)

Figure 11. Total displacement fields in the upper (a) and lower (b) parts of the analyzed structure.

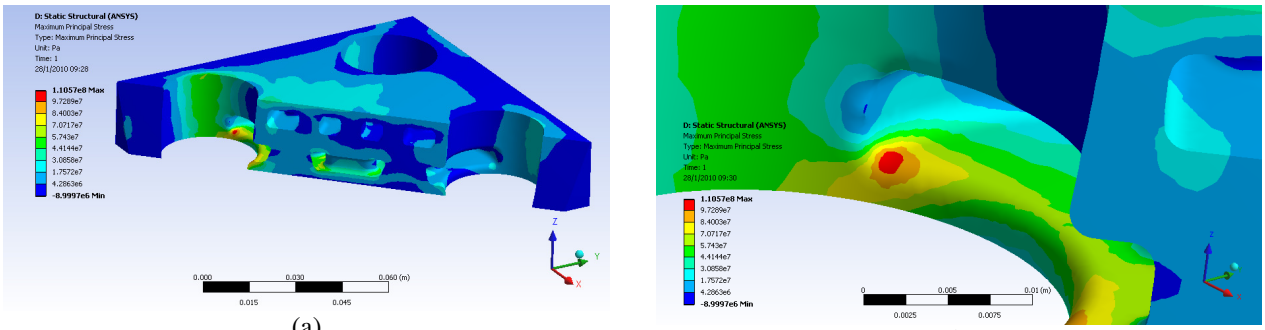

(a) (b)

Figure 12. Critical region identified near a rounded corner in terms of maximum principal stress (maximum value of σ_1 = 111.0 MPa - tensile stress).

Figure 13(a) presents the safety factors found for the heat exchanger using both discussed fracture criteria. It can be realized that in the studied case, due to the tensile largest normal stress (σ_1), both criteria present essentially the same results. For the most refined model considered, the safety factor is 2.41, which was considered adequate for the intended laboratory application. Figure 13(b) shows a contour plot of the safety factors found near the critical region.

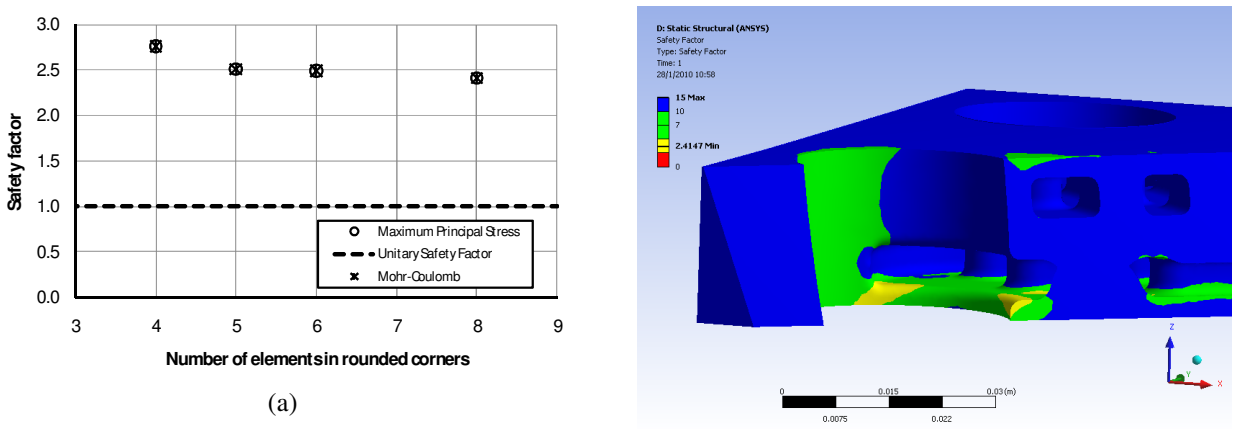

(a) (b)

Figure 13. Safety factors obtained considering Maximum Principal Stress and Mohr-Coulomb fracture criteria (a) and contour plot of the safety factors near the assessed critical region (b).

Though the obtained results were considered adequate for the proposed laboratory applications, real heat exchangers do not permanently operate under such controlled and stable conditions and should, in addition: i) include pressure and transient loadings and; ii) be assessed in terms of numbers of cycles for failure (fatigue life) looking for higher safety factors and structural integrity. As an example, recent studies conducted by Fischedick et al (2007) recommend a safety factor of 8 (considering only steady state conditions) and predicted fatigue life of 10^5 hours for a real EFCC heat exchanger.

7. CONCLUDING REMARKS

This work presented a procedure for the design of a ceramic heat exchanger of very small dimensions. In the future, the construction and test of the heat exchanger is intended, in order to validate the design methodology and gain further insight to extend it to practical applications.

The low effectiveness obtained with the design can be attributed to the cross flow configuration and low convective heat transfer coefficients resultant from laminar flow. The thermal resistance by conduction in the ceramic walls is not significant for the design simulated.

The thermo structural analyses provided a safety factor of 2.41, which is considered adequate for the proposed validation and laboratory applications.

Industrial heat exchangers, however, must consider additional loadings (such as pressure and transient thermal) and life-prediction methods.

8. ACKNOWLEDGEMENTS

The authors would like to acknowledge FEI for the research support.

9. REFERENCES

Sunden, B., 2005, High temperature heat exchangers (HTHE), Proceedings of Fifth International Conference on Enhanced, Compact and Ultra-Compact Heat Exchangers: Science, Engineering and Technology.

Kautz, M., Hansen, U., 2007, The externally-fired gas-turbine (EFGT-Cycle) for decentralized use of biomass, Applied Energy, Vol. 84.

Fischedick, J. S., Dreiβigacker, V., Tamme, R., 2007, An innovative ceramic high temperature plate-fin heat exchanger for EFCC processes, Applied Thermal Engineering, Vol. 27.

National Institute of Standards and Technology, 2010, "NIST Structural Ceramics Database", available at http://www.ceramics.nist.gov/srd/summary/scdaos.htm. Visited in January 28th 2010.

Manglik, R. M., Bergles, A. E., 1995, Heat transfer and pressure drop correlations for the rectangular offset strip fin compact heat exchanger, Experimental Thermal and Fluid Science, Vol. 10.

Dowling, N. E., 1999, Mechanical Behavior of Materials – Engineering Methods for Deformation, Fracture and Fatigue, second edition, Prentice Hall.

Anderson, T. L., 2005, "Fracture Mechanics: Fundamentals and Applications" – 3rd edition, CRC Press, New York.

Bathe, K., J., 1996, "Finite Element Procedures", Prentice Hall, New Jersey.

Kays, W. M., London, A. L., 1984, "Compact Heat Exchangers", 3rd edition, McGraw-Hill, New York.

10. RESPONSIBILITY NOTICE

The authors are the only responsible for the printed material included in this paper.